Poloxamer/sodium cholate co-formulation for micellar encapsulation of Doxorubicin with high efficiency for intracellular delivery: an *in-vitro* bioavailability study

Elisamaria Tasca[1,*], Patrizia Andreozzi[2,3], Alessandra Del Giudice[1], Luciano Galantini[1,4] Karin Schillén[5], Anna Maria Giuliani[6], Maria de los Angeles Ramirez[2], Sergio Moya[2,*], Mauro Giustini[1,4,*]

[1] Chemistry Department, University "La Sapienza", P.le Aldo Moro 5, 00185 Rome (Italy)

[2] Center for Cooperative Research in Biomaterials (CIC biomaGUNE), Basque Research and Technology Alliance (BRTA), Paseo de Miramon 182, 20014, Donostia San Sebastián, Spain

[3] Chemistry Department "Hugo Shiff", University of Florence, Via Della Lastruccia 13, Sesto Fiorentino, 50019 Firenze (Italy)

[4] Centre for Colloid and Surface Science - C.S.G.I. Operative Unit of Bari c/o Chemistry Department, University "Aldo Moro", Bari (Italy)

[5] Division of Physical Chemistry, Department of Chemistry, Lund University, P.O. Box 124, SE-221 00 Lund, Sweden

[6] STEBICEF Department, University of Palermo, Palermo (Italy)

*corresponding authors:

elisamaria.tasca@uniroma1.it - telephone: +39 06 4991 3179 - fax: +39 06 49913175

smoya@cicbiomagune.es – telephone: +34 943005311

mauro.giustini@uniroma1.it - telephone: +39 06 4991 3336- fax: +39 06 49913175

Abstract

Hypothesis

Doxorubicin hydrochloride (DX) is widely used as a chemotherapeutic agent, though its severe side-effects limit its clinical use. A way to overcome these limitations is to increase DX latency through encapsulation in suitable carriers. However, DX has a high solubility in water, hindering encapsulation. The formulation of DX with sodium cholate (NaC) will reduce aqueous solubility through charge neutralization and hydrophobic interactions thus facilitating DX encapsulation into poloxamer (F127) micelles , increasing drug latency.

Experiments

DX/NaC/PEO-PPO-PEO triblock copolymer (F127) formulations with high DX content (DX-PMs) have been prepared and characterized by scattering techniques, transmission electron microscopy and fluorescence spectroscopy. Cell proliferation has been evaluated after DX-PMs uptake for three cell lines (A549, Hela, 4T1). Cell uptake of DX has been studied by means of confocal laser scanning microscopy and flowcytometry.

Findings

DX-PMs formulations result in small and stable pluronic micelles, with the drug located in the apolar core of the polymeric micelles. Cell proliferation assays show a delayed cell toxicity for the encapsulated DX compared with the free drug. Data show a good correlation between cytotoxic response and a slow DX delivery to nuclei. DX-PMs offer the means to restrict DX delivery to the cell interior in a highly stable and biocompatible formulation, suitable for cancer therapy.

Keywords: drug-delivery; doxorubicin hydrochloride; PEO-PPO-PEO block copolymers; pluronics; bile salts; tumour cell lines; confocal microscopy

Introduction

Doxorubicin is one of the most effective anticancer agents in clinical use. However, doxorubicin based chemotherapy suffers from severe limitations due to important side effects, including cardiotoxicity and bone marrow suppression, and also multidrug resistance (MDR) arising from repeated or high-dose treatments.[1][2] A way to overcome these problems is to encapsulate doxorubicin into suitable carriers, which change the drug pharmacokinetics and lead to the targeted delivery of doxorubicin and to an increased drug latency time. Several carriers have been proposed for doxorubicin over the years.[3][4] Some of them are actively investigated and have already reached phase II/III clinical trials.[5][6]

To increase its solubility in water, doxorubicin is used in its hydrochloride form (DX). However, the water solubility of DX makes its encapsulation and controlled release from hydrophobic matrices difficult. The above-mentioned drug side effects and cytotoxicity require that the drug remains encapsulated during circulation and is released only once in the tumor environment. A potential means to increase DX encapsulation in a hydrophobic environment and avoid undesired release is its co-formulation with an organic anion that, by neutralizing its

charge, facilitate DXsolubilization in the hydrophobic domains of the hosting system. Among many potential carriers, those based on micelles have the advantages of the ease of preparation and of the capability to host hydrophobic drugs in the inner apolar domains of the micelle by polarity affinity. In particular, poloxamers, which are non-ionic triblock copolymers of polyoxyethylene or poly(ethylene oxide) (PEO) and polyoxypropylene or poly(propylene oxide) (PPO)[7][8][9] (Scheme 1), sometimes referred to by their trade names Pluronics® or Synperonics®, are highly appealing for drug encapsulation because of their high biocompatibility and the intrinsic stealth nature of the micelles formed.[10][11][12][13][14][15]

PEO-PPO-PEO triblock copolymers easily self-assemble, above a critical concentration (cmc) and critical temperature (cmt), to yield core-shell micelles,[16] where the hydrophobic core is formed by PPO and the hydrophilic corona by PEO. The hydrophobic molecules can be solubilized in the apolar core, while the hydrophilic ones are generally confined to the corona region. Amphiphilic molecules like bile salts can also be loaded mainly in the corona and at the core/corona interface.[17][18][19][20] To increase DX solubility into the micellar core we have recently prepared mixed micelles of the EO_{100}-PO_{65}-EO_{100} copolymer (F127), mixed with a corresponding amount of the bile salt sodium cholate (NaC).[21] The mixed micelles were loaded with DX, whose solubilization in the apolar core was driven by the interaction with the negatively charged cholate.[21] Indeed, the cholate salt is effective in increasing DX hydrophobicity and loading into the micelles thanks not only to the neutralization of electrostatic charges but also through hydrophobic interactions with the apolar moiety of DX as was proved by fluorescence lifetime studies.[21] Moreover, it has also been shown in the literature that bile salts enhance cells' sensitivity to DX.[22] In our previous work we did not perform cell studies. The concentration of DX tested was also not therapeutically relevant and the issue of removing the not encapsulated drug was not addressed.

Thus, in this work the protocol of DX encapsulation has been adapted to obtain a formulation therapeutically relevant, with all the drug locatedin the hydrophobic domains of the block copolymer micelle, and the therapeutic efficacy of the formulation has been tested in vitro.

Here we present a complete physico-chemical characterization and *in vitro* study of this new formulation whose main features are an 800 fold increase in the amount of drug compared with the original one,[21] without any free DX in the final product. Fluorescence spectroscopy, dynamic light scattering (DLS) and small angle X-ray scattering (SAXS) data revealed that the microstructure of the DX/NaC/F127 mixed micellar system was unaltered by the increased amount of drug even after the removal of free DX (denoted DX-PMs). The formulation has been successfully tested for its anticancer activity against three DX-sensitive cell lines using the 3-(4,5-Dimethyl-thiazol-2-yl)-2,5-diphenyl tetrazolium bromide (MTT) assay to measure cell viability. Confocal laser scanning microscopy (CLSM) and fluorescence flow cytometry were used to follow the uptake and intracellular colocalization of DX-PMs.

Materials and methods

Chemicals

NaC (≥ 99%), methanol (for HPLC; ≥ 99.9%), F127 copolymer (EO_{100}-PO_{65}-EO_{100} with nominal molecular weight of 12600 g/mol; BioReagent), 3-(4,5-Dimethyl-thiazol-2-yl)-2,5-diphenyl-

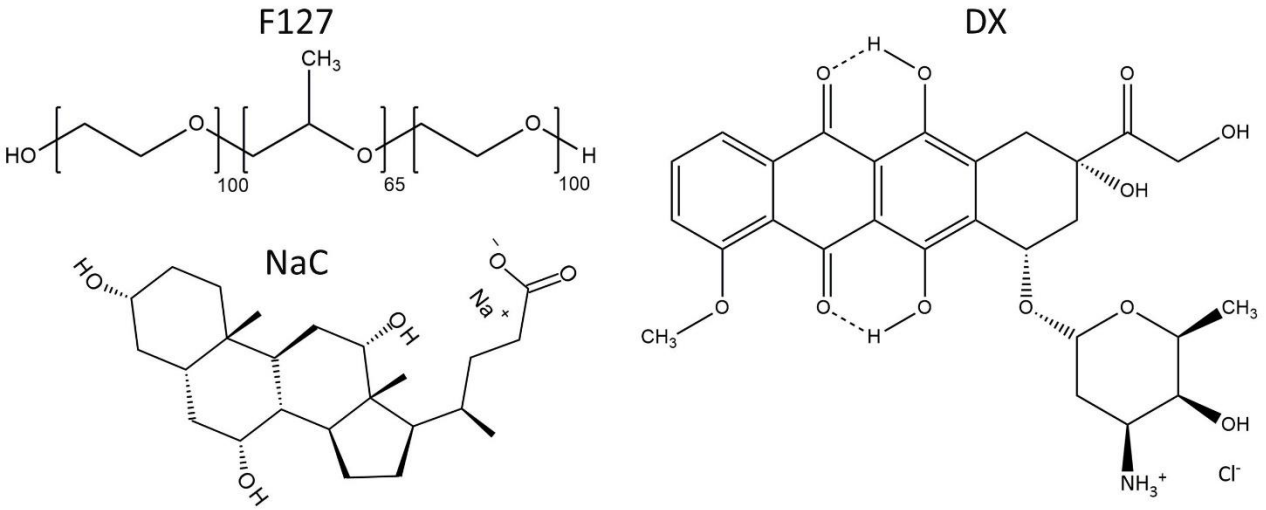

Scheme 1 Chemical formulae of the PEO-PPO-PEO block copolymer F127, the bile salt sodium cholate (NaC) and the antibiotic doxorubicin hydrochloride (DX).

tetrazolium bromide (MTT; 98%) and 2′-(4-Ethoxyphenyl)-5-(4-methyl-1-piperazinyl)-2,5′-bi-1H-benzimidazole trihydrochloride (Hoechst 33342; ≥ 98%) were purchased from Sigma-Aldrich. Doxorubicin hydrochloride (DX; ≥ 98%) was a kind gift of Farmitalia-Carlo Erba Chem. Co. Ultrapure water (18.2 MΩ/cm) from Arium pro UV system (Sartorius Stedim Biotech) was used in the preparation of the solutions. Penicillin–streptomycin antibiotic solution (P/S; 100 units/mL penicillin, 100 mg/mL streptomycin), Roswell Park Memorial Intitute-1640 (RPMI-1640), Dulbecco Modified Eagle Medium (DMEM), Leibovitz's L-15 Medium (L-15), Phosphate-buffered saline 10x, pH 7.4 (PBS), fetal bovine serum (FBS) and 0.25% (w/v) trypsin solution were purchased from Thermo-Fisher Scientific, USA. Human lung adenocarcinoma cells (A549), mammary carcinoma of mouse cells (4T1) and cervical cancer cells (HeLa) were purchased from the American Type Culture Collection (ATCC), USA. Culture plates and dishes were obtained from Corning Inc. NY, USA. Hamilton MidiPrep dialysis tubes were used with a cut off of 1000 g/mol. Calf thymus DNA (ct-DNA; 42% in GC base pairs) was obtained from Serva in vials of 250 mg and was used as received. A stock ctDNA water solution was prepared by dissolving 10.9 mg of the polynucleotide (average molecular weight $8.58 \cdot 10^6$ g/mol[23]) in 50mL ultrapure water; the resulting solution had an absorbance at 260 nm (ε_{260nm}= 6600 $M^{-1}cm^{-1}$[24]) of 0.425 (0.1 cm cell), from which a concentration (in phosphate groups) of $[ctDNA]_P = 6.44 \cdot 10^{-4}$ M was calculated.

Samples preparation

The DX/NaC/F127 mixed micelles were prepared as described.[21] Briefly, to mix the different species in their monomeric form, appropriate volumes of methanolic stock solutions of NaC and DX were mixed and F127 was then added as a solid. NaC and F127 were mixed to have a well-defined molar ratio MR (MR= n_{NaC}/n_{F127}). The amount of methanol necessary to obtain a clear solution (if needed) was added and then evaporated in a rotary evaporator followed by high vacuum pump. Ultrapure water, filtered through a 0.45 μm polycarbonate syringe filter (Millipore), was then added to reach a final F127 concentration of 1% (w/V), corresponding to a molar concentration of $7.9 \cdot 10^{-4}$ mol/L. In the final samples, the analytical concentration of both DX ($[DX]_{anal}$) and NaC was $1.6 \cdot 10^{-4}$ mol/L and, throughout this work, MR was fixed to 0.2 (this formulation has been already fully characterized in a previous work[21]). Samples were

first incubated overnight under gentle stirring at 4 °C and then 2 hours at 25 °C. Finally, the samples were kept in a thermostatic bath at 40 °C (a temperature above F127 cmt) under stirring in the dark and periodically checked for any variation in their fluorescence spectra. The solubilization of DX in the hydrophobic domain of the PMs was monitored following the intensity ratio ($R_F = I_1/I_2$) of the two well defined peaks in the emission spectrum of DX at 560 nm (I_1) and at 590 nm (I_2). Freshly prepared samples showed a $R_F \approx 0.8$ (typical of DX in a polar environment), which shifts with time towards the value of DX in an apolar environment ($R_F \approx$ 1.4 in *n*-hexane). [21][25] To remove non incapsulated DX, the samples were dialyzed (1 kDa membrane) in the presence of ctDNA at 40 °C under mild stirring. In detail, 800 µL of the DX/NaC/F127 mixed micelles at a certain time point from the sample preparation (see below) were introduced into a dialysis tube and dialyzed overnight against 50 mL of a solution containing NaC, F127 (at the same concentration as the samples) and a suitable volume of the ctDNA stock solution at a final molar ratio of $[ctDNA]_P/[DX]_{anal} = 6$. DX/NaC/F127 mixed micelles after the dialysis were denoted DX-PMs.

Physico-chemical characterization

DLS and ζ-Potential measurements were performed with a Zetasizer Nano ZS (Malvern Instruments Ltd., Worcestershire, UK) instrument, equipped with a 5 mW HeNe laser (λ= 632.8 nm) and a digital logarithmic correlator. The normalized intensity autocorrelation functions were measured at a fixed angle of 173°. The temperature was varied using the Peltier-thermostatted sample holder of the instrument (accuracy: ± 0.1°C). ζ-Potential measurements were performed with disposable folded capillary cells, DTS1070 (Malvern Instruments Ltd., Worcestershire, UK). All measurements were performed at 40 °C. Prior to the measurements, the solutions were equilibrated at 40°C for ten minutes. The reported ζ-Potential values are an average of three subsequent measurements. The errors are given ± standard deviation (SD). Steady state fluorescence measurements were performed with a Fluoromax 2 (Horiba-Jobin Yvon) spectrofluorometer using 0.3x0.3 cm black quartz cuvette from Starna GmbH. UV-Vis spectra were measured with a Varian Cary 5E instrument. Fluorescence lifetime measurements were performed with an home-build apparatus described in [21] with the only notable exception of the acquisition board, a Becker-Hickl SPC-130-EMN, that allowed a time resolution of 12.2 ps per channel (total channels acquired:4096) in the actual configuration. Being the IRF less than 90 ps and the DX lifetime at least one order of magnitude longer, the decays were fitted with a tailfit procedure as the sum of three or two exponential components depending on the incubation time from the preparation. The fitting procedure was performed by fixing the lifetime of the DX free in water to 1.00 ns and for the DX in the corona region of the polymeric micelles to 1.10 ns, as previously reported. [21] The lifetime of the slowest component, corresponding to the DX in the apolar core of the polymeric micelles was left as adjustable parameter: a lifetime of 4.01±0.10 ns was obtained. This value is slightly shorter than that found in our previous work (4.32±0.08ns) [21]; this small discrepancy is probably related to a closer packing of the DX due to its increased concentration in the apolar core of the PM in the present formulation.

For transmission electron microscopy (TEM) measurements, 6 µL of PMs and DX-PMs at 2 mg/mL kept at 40 °C under stirring prior to grid deposition, were transferred (3 µL at time) to

ultra-thin plasma coated carbon grids. Plasma negative discharge was applied on the surface of the carbon grid to make it hydrophilic (conditions: 25 mA, 2 min, $1x10^{-1}$ mBar). Each aliquot was incubated on the grid for 1 min to adsorb. After a drying step in which the drop was gently blotted with filter paper, grids were then washed with 3 µL of ultrapure water for 30 seconds and then water was removed by applying a filter paper. 3µL of $(NH_4)_2MoO_4$ (Sigma-Aldrich 99.98%; 2 % w/v, pH 6.5) staining solution was then added for 1.5 minutes and the excess removed by filter paper. Samples were washed twice with 3 µL ultrapure water and then air dried. TEM images were acquired with a LaB6-TEM JEM 1400PLUS (JEOL) microscope operating at an acceleration voltage of 100 kV.

SAXS measurements were performed using a laboratory based Xeuss 2.0 HR P300K Q-Xoom system (Xenocs SAS, Grenoble, France), having a micro-focus Genix 3D X-ray source with λ = 0.154 nm and a two-dimensional Pilatus3 R 300K detector from Dectris (Dectris Ltd., Baden, Switzerland). The samples were characterized in sealed quartz capillaries with thickness of 1.5 mm kept at 40 °C. Measurements were performed at reduced pressure (< 0.2 mbar), with two different sample-detector distances, in order to record the sample scattering within the q range 0.045 nm^{-1} < q < 6.2 nm^{-1}, where $q = 4\pi \sin(\theta) / \lambda$, 2θ being the scattering angle. Water was used to collect the background data for subtraction. The SAXS data reduction (radial averaging, background subtraction, absolute intensity scaling) was performed using the FoxTrot software developed at SOLEIL. Pair distance distribution functions and Guinier fits were obtained by using the ATSAS package. [26] Model scattering profiles were calculated and fitted to the data with the software SasView. [27]

Cell culture

A549 and 4T1 cell lines were cultured with RPMI-1640 supplemented with 10 % (v:v) FBS and 1% (v:v) P/S antibiotic solution. HeLa cells were cultured with DMEM supplemented with 10 % (v:v) FBS and 1% (v:v) P/S. Cells were maintained at 37 °C, 5% CO_2 in a humidified chamber.

Cell viability MTT assay

The cytotoxicity of the PMs without DX was tested in three different cancer cell lines: A549, 4T1 and HeLa. The cells were grown on 96-well microplates to a density of 10 x 10^3 cells per well. Cell mitochondrial activity was tested using the MTT assay which is based on the mitochondrial conversion of tetrazolium salt into a formazan dye with absorption characteristics in the visible region. PMs with and without DX were incubated with cells at different concentrations (from 0.03 to 3.2 µM of DX corresponding to the range between 0.02 and 3 mg/mL of PMs) and different time points (3, 24 and 48 h). Following incubation with PMs, at each time point cells were washed with PBS, and 135 µL of fresh medium with 15 µL MTT at 5 mg/mL in PBS was added to each well. Culture plates were then incubated at 37 °C. After 2 h of incubation, medium-containing MTT was discarded and formazan crystals were dissolved in 150 µL DMSO. The absorbance at 550 nm, with automatic correction at reference wavelength 630 nm, of the resulting solution was measured in a 96-well spectrophotometer microplate reader. The percentage of cell mitochondrial activity ($MA_{\%}$) was determined as:

$$MA_{\%} = \frac{Abs_{treated}}{Abs_{control}} \cdot 100$$

Cellular uptake of PMs in different cancer cell lines

The cellular uptake of DX-PMs in three different cancer cell line (4T1, A549 and HeLa) were quantified by flow-cytometry (BD-FACs Canto II cytometer, Becton Dickinson, USA). Free DX and not loaded PMs were used as controls. Briefly, 15 x 10^3 cells were cultured in 48-well plates until a density of 30 x 10^3 cells per well after 24 h and exposed to 1.5 mg/mL of DX-PMs or 1.6 μM of free DX at different times, from 0.25 h to 24 h at 5 % CO_2 and 37 °C. Then, cells were washed with PBS and 50 μL trypsin was added. An additional 150 μL PBS was added to neutralize trypsin and finally cells were transferred to FACS tubes for analysis. Fluorescence of the cells was quantified and analysed by FACS. Measurements were performed in duplicate and approximately 10000 events (cells)/sample were analysed. The mean fluorescence intensity obtained was normalized respect to the autofluorescence of untreated cells (this last parameter was used as a control) to be directly related to the amount of drug within the cells.

Cell entry mechanism and intracellular trafficking of PMs

10 x 10^3 cells per well were plated in 8-well ibidi μ-slide chambers (ibidiTreat) in 200 μL of medium with 10 % of FBS and 1 % P/S and incubated at 37 °C for 24 hours. Before cellular uptake experiments, cells were washed with 200 μL fresh medium and then 1.5 mg/mL of DX-PMs were added to the well. 1.6 μM solution of free DX was used as a positive control. Cells not treated were used as a control. After the desired incubation time (0.5, 3, 16, 24 and 48 h) cells were washed twice with fresh medium. In all cases, cells nuclei were counterstained with HOECHST 33342 dye, diluted 1:1000 with full medium from a water stock solution containing 10 mg/mL of dye, for 5 minutes at 37 °C. Excess dye was washed with fresh medium and confocal experiments were performed in L-15 medium containing 10% FBS and 1% P/S. CLSM imaging was performed exciting at both 405 and 488 nm excitation laser lines, with a 63x oil immersion objective. All images were acquired with a CLSM 510 Zeiss laser scanning microscope. To evaluate the uptake of DX into the nucleus, fluorescence intensity scan profiles were taken by random sampling by tracing a vector across the cell length and the values obtained plotted as fluorescence emission graphs using Zen 3.1 (ZEN lite) microscope software from ZEISS Microscopy.

Results and discussion

Structural characterization of PMs and DX- PMs

TEM of DX-PMs shows a monodisperse population of small-sized spherical micelles with an apparent average diameter of 30 nm (Figure 1- panel a). Indeed, a core-shell structure of the DX-PMs is shown by the TEM image at higher magnification (Figure 1- inset of panel a). No significant differences in the size of DX/NaC/F127 mixed micelles before and after dialysis were detected with DLS data (Figure 1 - panel b). A hydrodynamic diameter (D_H) of 28.3 ± 0.6 nm and a polydispersity index (PDI) of 0.21 were calculated for both samples by the CUMULANT analysis of the relevant autocorrelation functions. The structure of empty PMs shares the same main features of DX-PMs in terms of dimensions and core-shell structure (see Appendix, Figure A1 –panel a). These results are in excellent agreement with those obtained by DLS for this system (Figure A1 –panel b). The D_H of empty PMs is 25.7 ± 0.4 nm (Figure A1 –panel b) with a PDI of 0.25. The ζ-potential value measured for the empty PMs is slightly negative (-13.7 ± 0.9 mV), while for the DX-PMs the ζ-potential rises to -4.7 ± 0.5 mV, in agreement with the presence of the cationic DX in the corona region of the micelles. In terms of both size and structure, no significant differences can be appreciated between PM and DX-PMs. SAXS measurements of pre- and post-dialysis samples were performed (Figure 1 – panel c). They outline the presence of spherical block-copolymer micelles with a compact core of 9.3 nm diameter and a shell of polymeric chains, for a total maximum particle diameterof 22 nm (see Appendix, Figure A2 and Table A1). The size isslightly larger than those inferred from SAXS data on pure F127 micelles[18] thus supporting the loading of NaC and DX. Both DLS and SAXS confirmed that after dialysis the DX-PMs preserve their original dimensions as well as their core-shell structure.

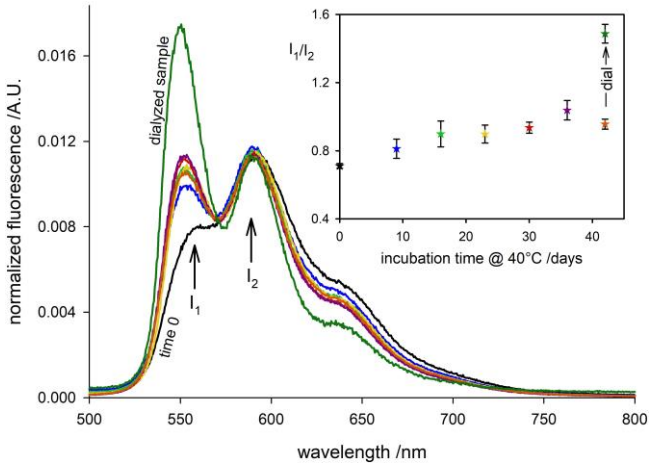

Figure 2 Fluorescence emission spectra of DX in the DX/NaC/F127 mixed micelles as a function of incubation time at 40°C. After 42 days samples were dialyzed to remove the free drug (green line). The inset shows the evolution of the fluorescence intensity ratio (I_1/I_2 – arrows in the main graph) as a function of the incubation time at 40 °C (before and after dialysis for the sample at 42 days of incubation time -green colour; see text for details). Error bars represent the SD (n= 4).
$[DX]_{anal}$= 1.60·10^{-4} M; [F127]= 7.9·10^{-4} M; [NaC]= 1.60·10^{-4} M; λ_{exc}= 410 nm; slits: 1.75/1.75 nm; 0.3x0.3 cm cell; T= 40°C.

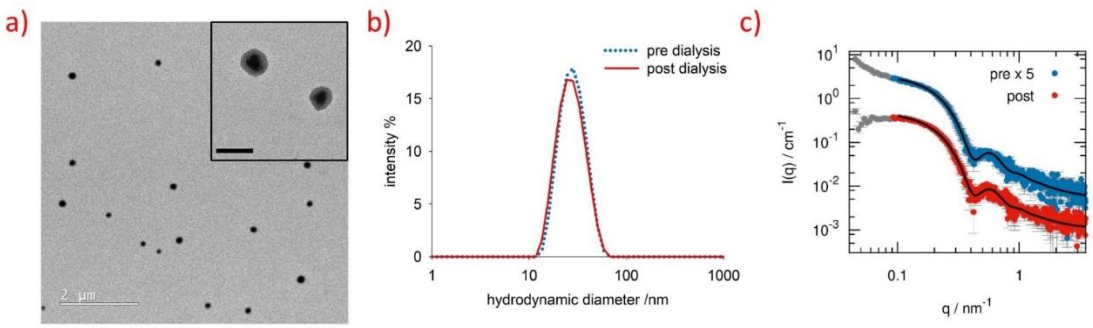

Figure 1 a) TEM images of DX-NPs (scale bar in the inset indicates 200 nm). **b)** DLS data of DX/NaC/F127 mixed micelles in aqueous solution at 40°C before (blue dotted line) and after (red line) dialysis. **c)** SAXS data of the same samples as in panel b) (dots) and best fitting curves (black lines) with the form factor of spherical particles with a compact core and a shell of polymeric chains (see Appendix).

Steady-state fluorescence emission spectra (Figure 2) revealed that increasing the incubation time at 40 °C results in an increase in the R_F ratio (Figure 2 – inset).
This result indicates the progressive migration of the drug into the apolar core of PMs, and it is in perfect agreement with previous data of DX-PMs at a lower drug concentration.[21] After 43 days, however, the ratio is still far from the typical R_F value of DX in an apolar environment, suggesting that a significant amount of DX is present in the corona region of the polymeric micelles. Indeed, time resolved fluorescence spectroscopy (Figure 3) revealed that after 43 days only 54±4.1 % (Figure 3 – inset) of the drug displayed a lifetime typical of DX in the inner apolar compartment of PMs (τ_{slow}= 4.01±0.10 ns), with the remaining DX located in the corona as inferred from the lifetime (τ_{fast}= 1.10 ns). [21] The process of DX solubilization in the NaC/F127 PM results first in an accumulation of the drug in the corona region and then its translocation to the less polar micellar compartment (Appendix, Figure A3). To remove the more mobile fraction of DX in the corona region of PM, the samples were dialyzed against a ctDNA solution (see Materials and Methods) taking advantage of the high association constant between DX and DNA (as high as 10^6 M^{-1}).[28] The use of ctDNA as a DX sequestrant allowed a quantitative removal of non-entrapped DX in a single dialysis step (see Appendix, Figure A4.1 and A4.2 for details).
Once formed, DX-PMs remain stable even to freeze-drying, changing of buffer, and exposure to extremely acidic pHs, without releasing the entrapped drug.[21] Due to this high stability, the dialysis procedure led to DX-PMs without any detectable free drug, as revealed by both steady-state (Figure 2) and time resolved (Figure 3) fluorescence. These dialyzed DX-PMs were then freeze-dried ato be later resuspended in a suitable media for testing their activity *in vitro*. It is important to remark that, once resuspended in water after lyophilization, DX-PMs showed the same characteristics of the non lyophilized systems, in agreement with the previous findings at much lower drug concentration.[21]
The loading efficiency of the DX-PMs was evaluated using the superposition along 10 nm wavelength interval (centred at 518 nm) of the absorption spectra of free DX and DX-PMs (Appendix, Figure A5). It was then straightforward to calculate the loading efficiency, $L_{\%}$ (expressed as moles percent), as

$$L_{\%} = \frac{Abs_{after}^{518\,nm}}{< Abs_{pre}^{518\,nm} >} \cdot 100$$

(where $Abs_{after}^{518\,nm}$ is the absorbance measured at 518 nm after the dialysis while $< Abs_{pre}^{518\,nm} >$ refers to the average of the absorbances at 518 nm measured for all the spectra acquired before dialysis - details on this procedure are given in Figure A5). Depending on samples and incubation time at 40°C, loading efficiency values as high as 30% were

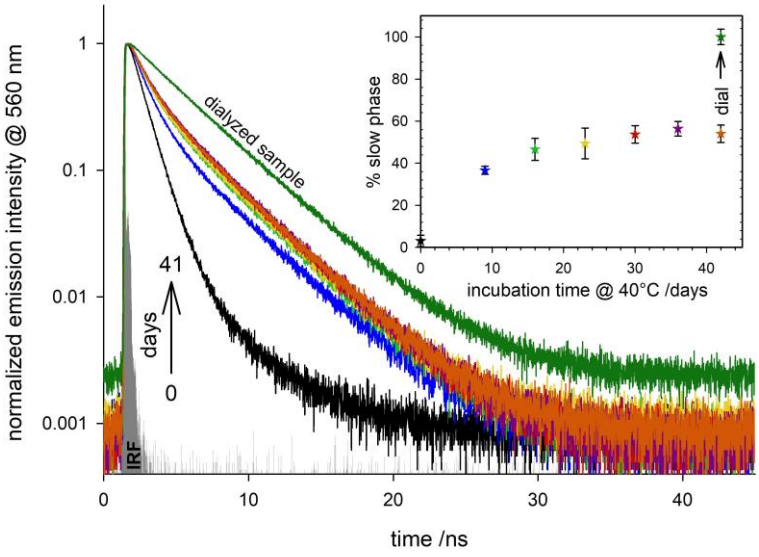

Figure 3 TCSPC decays (measured at 40°C) of DX in the DX/NaC/F127 mixed micelles (same sample as in Figure 2) as a function of incubation time at 40°C before and after dialysis to remove the drug in the corona region of PM (dark green line). The inset shows the evolution of the slow phase (τ_{slow}= 4.01±0.10 ns) percentage with time before and after dialysis (dark green symbol). Error bars correspond to the SD (n= 4).

obtained. From $L_{\%}$ it was possible to calculate the drug loading ($DL_{\%}$) as weight percent, according to:[29]

$$DL_{\%} = \frac{g_{DX_{in}}}{g_{DX_{in}} + g_{NaC} + g_{F127}} \cdot 100$$

where $g_{DX_{in}}$is the mass of DX incorporated in the polymeric micelles (obtained from UV-Vis measurements; making reference to 1.0 L of DX-PM: $g_{DX_{in}} = 2.61 \pm 0.1 \cdot 10^{-2} g$) and g_{NaC} and g_{F127} are the mass of all the other species present in the dispersed micellar phase (making reference to 1.0 L of DX-PM: $g_{NaC} = 9.95\ g; g_{F127} = 6.80 \cdot 10^{-2} g$). A $DL_{\%}$ of 0.26±0.14 % was obtained, values not far from those reported in the literature for polymeric micelles made of poly-lactide-co-glycolic acid and the anthracycline epirubicin.[30]

To compare the *in-vitro* results obtained with DX and DX-PMs, water solutions of free and encapsulated drug having the same absorbance at 518 nm were prepared and then suitably diluted as described in the Materials and Methods section.

Cell viability assay

One of the aims of this study was to evaluate the *in vitro* cytotoxicity of DX-PMs in comparison with that of free DX. Cell viability was evaluated in three different cancer cell lines: A549, 4T1 and HeLa cells each having different sensitivities to DX. HeLa [31][32][33] and 4T1 [34][35] are the most DX-sensitive cancer cell lines, while A549 is significantly more resistant.[36]

To evaluate PMs toxicity, the three cell lines were incubated in solutions with high PM concentrations ranging from 0.75 to 3 mg/mL, and for long times up to 48 h. Cell viability remained well above 80% even in the most unfavourable conditions tested (Figure A1 – panel c).[23][37] This high cytocompatibility of the PMs allowed us to correlate any cell toxicity of DX-PMs detected as a function of DX release into the nucleus.

The cytotoxicity profiles of free DX and DX-PMs were evaluated in the three different cell lines by the MTT assay. Cells were treated with different concentrations of free DX and of DX-PMs and incubated for 3 (Appendix, Figure A6), 24 and 48 h (Figure 4). It can be observed that cell proliferation rate depends on both drug concentration and incubation time and the trend in cell viability is different for each cell line (Figure 4). For all cell lines tested, free DX is more toxic than DX encapsulated into PMs, which is particularly evident after 48 h of incubation. These differences in cytotoxicity between DX and DX-PMs may be due to the different cellular trafficking mechanisms of DX. The free drug is passively absorbed by diffusion into the cell, whereas DX-PMs are incorporated by an endocytosis mechanism where DX-PMs are released from the endosome to the cytosol and finally DX reaches the nucleus.[38][39] This difference implies a faster DX diffusion to the cell nuclei in the case of free drug, and a delayed delivery of DX to the nuclei in the case of the DX-PMs. This slow kinetic mechanism of DX reaching the nucleus results in the observed time-dependent cell-growth inhibition.

The cell viability of DX-PMs in a cell line less sensitive to DX, such as A549 cells[36], remains above the half maximal inhibitory concentration (IC_{50}) up to 48 hours (Figure 4 – panel a) while at the highest free DX concentrations the cell viability was below to the IC_{50}. A different viability profile is observed in HeLa [31][32] (Figure 4 – panel b) and 4T1 [40] (Figure 4 – panel c) cell lines. These cells are markedly sensitive to free DX even at low concentrations and at short exposure times. A viability below IC_{50} is seen after 3 h of exposure to high DX concentrations for HeLa and 4T1 cell lines (Appendix, Figure A6 - panels b, c), while for A549 the viability remains around IC_{90} (Appendix, Figure A6 – panel a). Depending on the DX concentration, at 24 and 48 h there is a generalized dramatic decrease in cell viability that reaches values close to zero. A significant difference between the cytotoxicity profiles of free DX and DX-PMs in these two cell lines is evident and becomes clearer at high drug concentrations and long incubation times. The cellular uptake of DX-PMs shows, in both cell lines, a slightly reduced toxicity profile, mainly at lower concentrations (from 0.03 μM to about 0.1 μM DX-PMs) compared with free DX. Cell viability is above 50% even after long exposure (Figure 4 – panels b and c). At higher concentrations, from 0.2 μM to about 3 μM DX-PMs, toxicity is significantly reduced compared to the free drug by a factor of ~2 (Figure 4 – panels b and c). These data confirm that A549 cells are resistant to DX (both as free drug and in DX-PMs)[36] compared with the other cell lines investigated. However, DX toxicity is significantly reduced when DX is encapsulated into the mixed micellar nanoparticles. Such an effect can be rationalized by taking into consideration the above-mentioned different uptake mechanism for the free DX and DX loaded into PMs. As described below, we support this reasoning with results from cellular uptake studies performed with CLSM

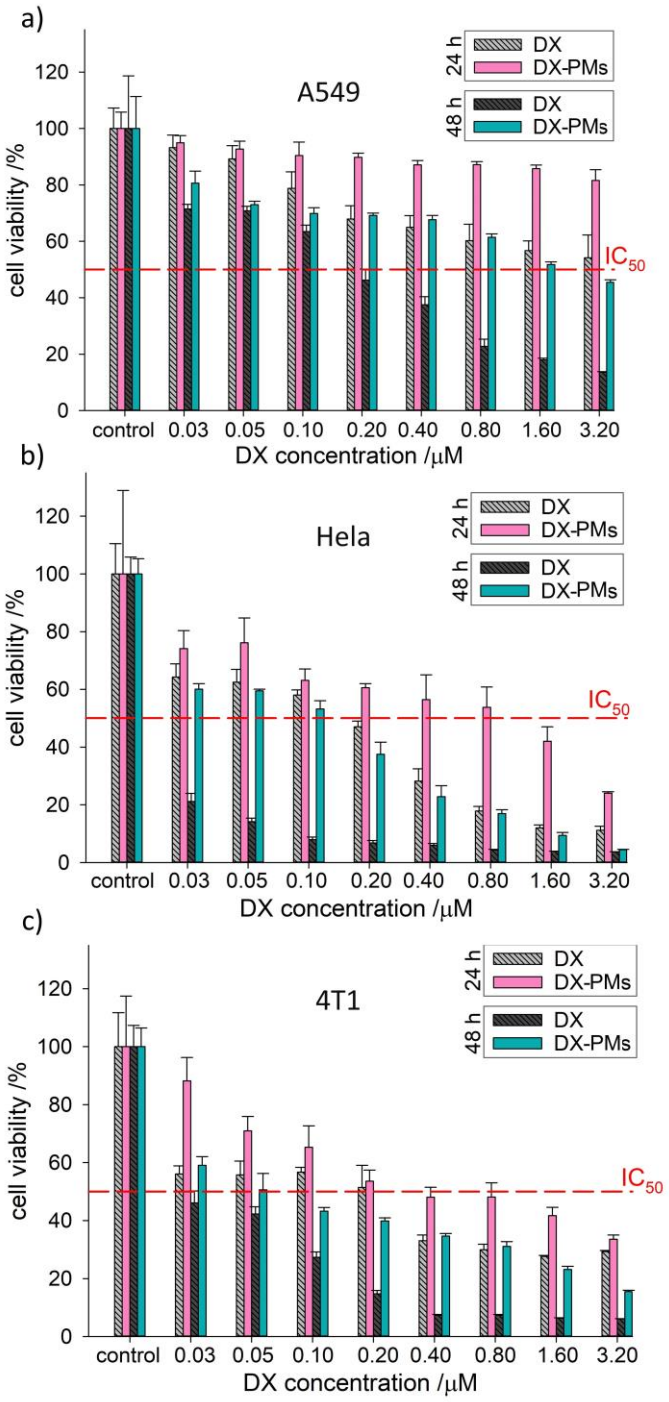

Figure 4 MTT assay results for three different cell lines: **a)** A549; **b)** HeLa; **c)** 4T1. All cells were treated with free DX and DX-NPs at different concentrations obtained by scalar dilutions and at different incubation times at 37°C. Error bars represent the standard deviation (n=9).

cellular uptake of free DX and DX-PMs

The intrinsic fluorescence of DX allowed the use of flow cytometry and confocal fluorescence microscopy to study the cellular uptake and intracellular localization for both free DX and DX-PMs. Experiments were performed at a drug concentration of 1.6 μM. This value was chosen as a compromise between a cytotoxic DX dose do not leading to the complete cell death at long exposure times and the amount of drug allowing a good DX fluorescence signal for both free DX and DX-PMs. Nuclei were stained with HOECHST dye (blue fluorescence signals in CLSM images) and free DX and DX-PMs are indicated by green fluorescence signals. The three cell lines exhibited similar patterns of cell distribution of DX and DX-PMs and the differences in the fluorescence intensity of DX between the cytoplasm and the nuclei can be well appreciated (Figure 5). After 30 min, it is evident from CLSM that DX-PMs are readily incorporated into the cells, independently of the specific cell line investigated (compare panels a, b and c in Figure 5

at 0.5 h of exposure time) and more markedly than free DX, as confirmed by flow cytometry data (Figure 6). However, while the DX fluorescence in the nuclei is readily detected in the first 3 h after exposure in free DX treated cells, no DX fluorescence can be detected in the nuclei of cells treated with DX-PMs up to 16 h. Additional confocal images taken at longer incubation times (24 and 48 h) in 4T1 cells show that after 24 h DX moves into the nucleus (Figure 7). Drug accumulation in the nucleus starts to become evident after 24 h of uptake of DX-PMs in all three cell lines explored. In particular, the line-scanning profiles of fluorescence derived from the CLSM images show that the DX fluorescence signal overlaps with that of dye staining the nucleus (HOECHST) already after 24 h. At 48 h a very intense DX signal can be appreciated in

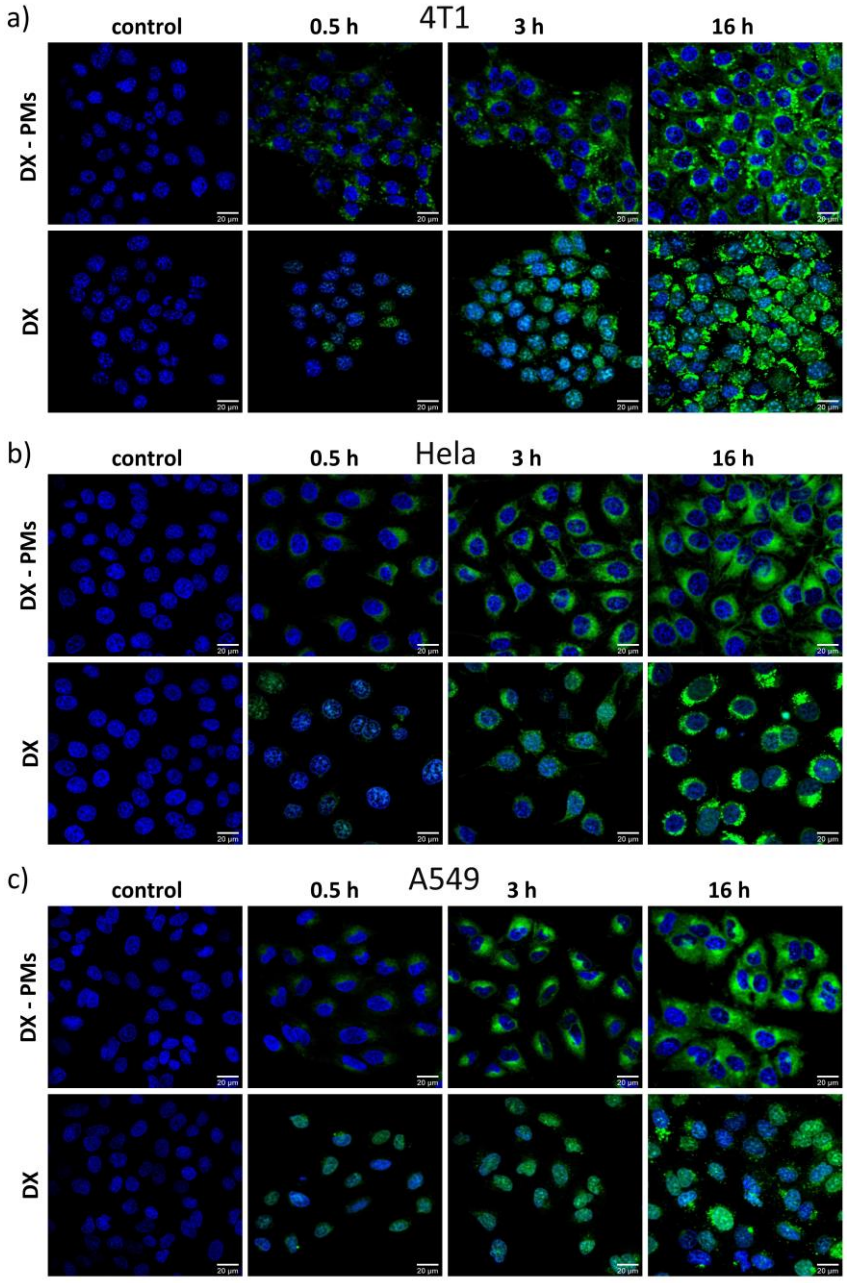

Figure 5 CLSM micrographs showing cellular uptake of DX-NPs (upper panels) and free DX (bottom panels) at different incubation times for **a)** 4T1, **b)** HeLa and **c)** A549 cell lines. The concentration of DX (free DX and DX NPs) in the cell culture was 1.6 μM. Scale bar: 20μm. Nuclei are stained with HOECHST dye (blue signal), and DX or DX-NPs are indicated by green signal.

the nuclear region, almost totally masking that of HOECHST. In agreement with the internalization profile observed in the 4T1 cell line, the internalization of DX-PMs in the HeLa cell line also shows a similar trend (Appendix, Figure A7.1). In A549 cells (Appendix, Figure A7.2), a similar behaviour can be appreciated but with a DX signal of lower intensity in the nucleus at 24 h, that increases at longer times, in line with the less sensitivity of this cell line to DX. The differences in drug uptake for free DX and DX-PMs are also evidenced by the flow cytometry data reported at different incubation times for the three cell lines investigated (Figure 6). At short incubation times, the fluorescence intensity of DX-PMs is almost the double compared with the mean fluorescence intensity of free DX. A very similar uptake level is observed for 4T1 and HeLa cells, while A549 cells show a less efficient internalization of both DX and DX-PMs, even at longer incubation times (Figure 6). These results are in good agreement with CLSM data, which also show that the internalization efficiency of DX-PMs is higher than that of free DX. The increase in the amount of drug detected at short times within the cells for DX-PMs, is not coupled to a decrease in cell viability, which can be explained as a consequence of the slow release of the drug from DX-PMs when inside the cells. The lag time between the accumulation of free and encapsulated DX in the nucleus results from the different uptake mechanism of free DX and DX-PMs by the cells [41][42]. It has been reported in the literature that poloxamer-based drug delivery systems enter cells through endocytosis [43][44][36]. An initial endosomal confinement of DX-PMs can be assumed before translocation and accumulation in the cytoplasm. The lag time of DX-PM is compatible with an endocytosis mechanism of entry , which is followed by the release of DX from the micelles before the drug can reach the nucleus. This hypothesis is confirmed by the results from the MTT assay, which show a delayed cytostatic

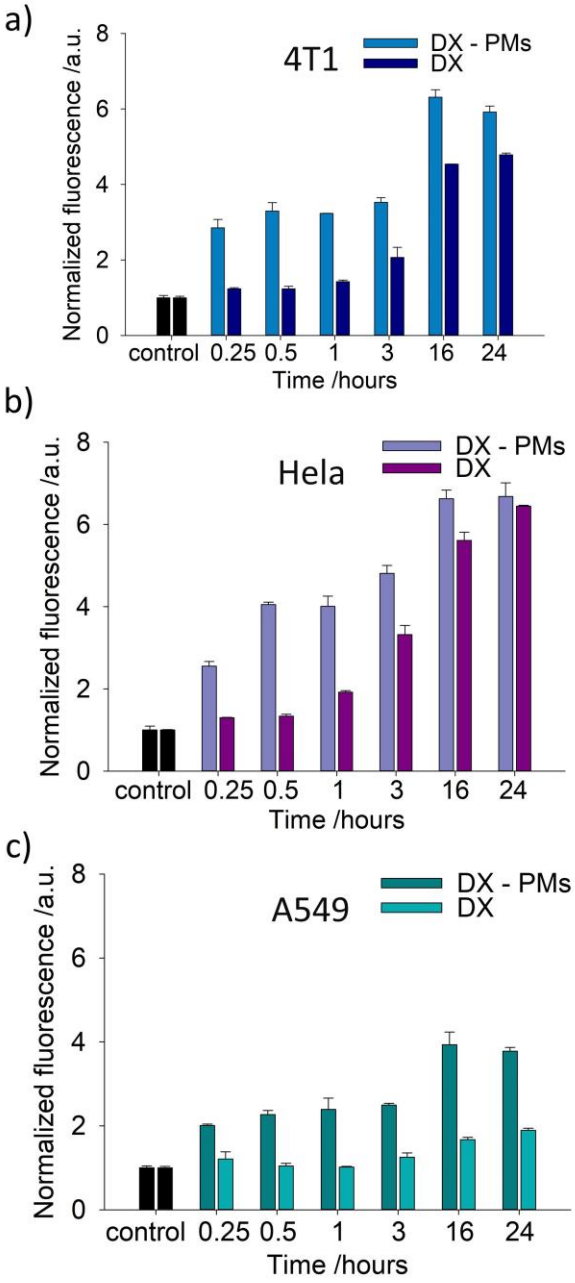

Figure 6 Fluorescence flow cytometry mean fluorescence intensity (normalized respect to the autofluorescence of untreated cells - used as a control) as a function of exposure time to free DX and DX-NPs by the cells: **a)** 4T1, **b)** HeLa and **c)** A549 cell lines. The concentration of DX (free DX and DX NPs) in the cell culture was 1.6 μM. The bar represents the standard deviation (n=2).

effect of DX. In the case of free drug, the rapid entry into the cytoplasm by diffusion is immediately followed by the translocation of the molecule into the nuclei with a prompt cytotoxic effect. In the case of DX-PM, the cytotoxic effect is delayed at short time, but drastically enhanced at long time [36][43][44]. Encapsulation of DX in polymeric micelles leads to a slow diffusion of DX over time to the nucleus, as has been reported for other DX delivery systems [38]. It might be also considered that the interaction of DX with the NaC probably plays a role in the slower diffusion of DX. The interaction of DX with NaC could hinder the translocation from the cytoplasm to the nucleus, as the DX should not be complexed to NaC to interact with the negatively charged nucleic acids, although further experiments would be needed to confirm or reject this possibility. From the confocal data of Figure 5, the lag time from cellular penetration to diffusion to nuclei can be estimated to be as long as 16 h for all the cell lines investigated. Since free DX penetrates the cells through simple diffusion through the plasma

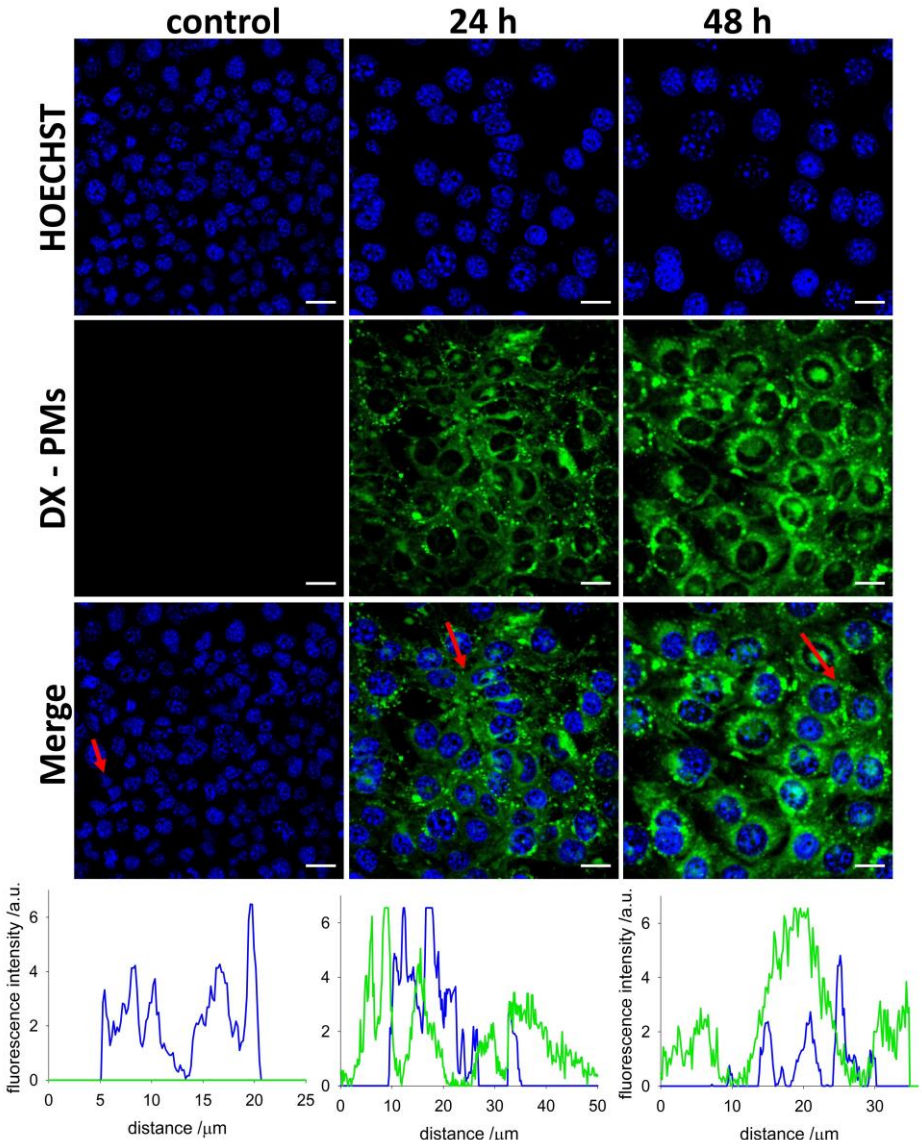

Figure 7 CLSM micrographs showing cellular uptake of DX-NPs in 4T1 cell line at two different incubation times. The concentration of DX-NPs in the cell culture was 1.6 μM. Nuclei are stained with HOECHST dye (blue), and presence of DX-NPs is shown by green fluorescence. Scale bar: 20 μm. The positions where the line-scanning profiles of fluorescence intensity of the cells (lower graphs) have been taken are indicated by the red arrows. In the fluorescence intensity plots the blue line indicates signal from HOECHST, and the green line signal from DX.

membrane, a detected fluorescence emission inside the nucleus with little signal in the cytosol is also observed at short exposure time, already after 3 h. This fast accumulation of DX into the nucleus is responsible for the decrease in cells' viability observed with the MTT assay. A very similar internalization trend of free DX and DX-PMs is observed for all three cell lines investigated (Figure 5).

Conclusions

In this study, the amphiphilic poloxamer F127 co-formulated with the bile salt NaC was employed as a nanocarrier to deliver DX in cancer therapy. DX-PMs were found to have a uniform core-shell structures with a particle size around 28 nm with a total drug loading efficiency of up to 30%. Unloaded PMs show high cytocompatibility. The therapeutic efficacy of the DX-PMs was evaluated by measuring cell viability in three cancer cell lines with different DX resistance. In all cases, cell viability decreased with DX-PMs but at a slower rate than for free DX. Cell viability results can be well correlated with the CLSM study of DX intracellular fate. While free DX accumulates rapidly in the nuclei, the release profile of DX-PMs in the three different cell lines was found to be time dependent, with an early internalization of DX-PMs into the cytoplasm and subsequent slow drug release into the nucleus. Our results show that the strategy of co-formulating poloxamer F127 with the bile salt NaC provides a means to encapsulate DX (by electrostatic/hydrophobic interaction with the bile salt) in a cytotoxic relevant dose and enables control of intracellular DX release. The formulations have high stability, with non-measurable release of the encapsulated DX outside the cell. Furthermore, DX-PMs have a size compatible with the enhanced permeability and retention (EPR) effect. The stability and size of DX-PMs therefore makes them particularly well-suited for use in cancer therapy with potential for tumour selectivity and DX delivery limited to the intracellular milieu.

Further work will focus on investigation of the extremely slow kinetics of DX solubilization and the exact localization of the drug in the NaC/F127 polymeric micelles by means of 2D-NMR techniques [45]. From the biological point of view, our efforts are currently dedicated to establishing the exact mechanism of entry of DX-PMs in the cells by labelling with suitable fluorescent dyes both the polymers and the NaC. Moreover, in the attempt to ameliorate the loading efficiency of our drug-delivery system we are exploring bile salts and pluronics with different hydrophobic/hydrophilic balance, which is expected to play an important role in the ability of the carrier to uptake and release the drug. Other drugs and pharmacologically active species are in the meanwhile being investigated as guest molecules.

Acknowledgements

We acknowledge the SAXSLab Sapienza facility at Sapienza University of Rome for the SAXS measurements. This work benefited from the use of the SasView application, originally developed under NSF award DMR-0520547. SasView contains code developed with funding from the European Union's Horizon 2020 research and innovation programme under the SINE2020 project, grant agreement No 654000.

M. Giustini and E. Tasca kindly acknowledged the financial support of Sapienza University (Progetti avvio alla ricerca 2018 and 2019).

K. Schillén kindly acknowledges the Sapienza Visiting Professor Programme 2018 for the visiting professorship grant.

S. Moya and P. Andreozzi thank the MAT2017-88752-R Retos project from the Ministerio de Economía, Industria y Competitividad, gobierno de España. This work was performed under the Maria de Maeztu Units of Excellence Program from the Spanish State Research Agency – Grant No. MDM-2017-0720. We also thank Dr. Julia Cope, PhD at CIC biomaGUNE, for revising the manuscript.

Bibliography

[1] M. Mohajeri, A. Sahebkar, Protective effects of curcumin against doxorubicin-induced toxicity and resistance: A review, Crit. Rev. Oncol. Hematol. 122 (2018) 30–51. doi:10.1016/j.critrevonc.2017.12.005.

[2] H. Cortés-Funes, C. Coronado, Role of anthracyclines in the era of targeted therapy, Cardiovasc. Toxicol. 7 (2007) 56–60. doi:10.1007/s12012-007-0015-3.

[3] G. Minotti, P. Menna, E. Salvatorelli, G. Cairo, L. Gianni, Anthracyclines: Molecular Advances and Pharmacologic Developments in Antitumor Activity and Cardiotoxicity, Pharmacol. Rev. 56 (2004) 185–229. doi:10.1124/pr.56.2.6.185.

[4] R. Danesi, S. Fogli, A. Gennari, P. Conte, M. Del Tacca, Pharmacokinetics-Pharmacodynamic Relationships of the Anthracycline Anticancer Drugs, Clin. Pharmacokinet. 41 (2002) 431–444.

[5] L. Giodini, F. Lo Re, D. Campagnol, E. Marangon, B. Posocco, E. Dreussi, G. Toffoli, Nanocarriers in cancer clinical practice: a pharmacokinetic issue, Nanomedicine Nanotechnology, Biol. Med. 13 (2017) 583–599. doi:10.1016/j.nano.2016.07.012.

[6] M. Cagel, E. Grotz, E. Bernabeu, M.A. Moretton, D.A. Chiappetta, Doxorubicin: nanotechnological overviews from bench to bedside, Drug Discov. Today. 22 (2017) 270–281. doi:10.1016/j.drudis.2016.11.005.

[7] A.M. Bodratti, P. Alexandridis, Formulation of poloxamers for drug delivery, J. Funct. Biomater. 9 (2018) 11. doi:10.3390/jfb9010011.

[8] Y. Zhang, W. Song, J. Geng, U. Chitgupi, H. Unsal, J. Federizon, J. Rzayev, D.K. Sukumaran, P. Alexandridis, J.F. Lovell, Therapeutic surfactant-stripped frozen micelles, Nat. Commun. 7 (2016) 1–9. doi:10.1038/ncomms11649.

[9] P. Alexandridis, T. Alan Hatton, Poly(ethylene oxide)-poly(propylene oxide)-poly(ethylene oxide) block copolymer surfactants in aqueous solutions and at interfaces: thermodynamics, structure, dynamics, and modeling, Colloids Surfaces A Physicochem. Eng. Asp. 96 (1995) 1–46. doi:10.1016/0927-7757(94)03028-X.

[10] M. Cavadas, Á. González-Fernández, R. Franco, Pathogen-mimetic stealth nanocarriers for drug delivery: A future possibility, Nanomedicine Nanotechnology, Biol. Med. 7 (2011) 730–743. doi:10.1016/j.nano.2011.04.006.

[11] K. Knop, R. Hoogenboom, D. Fischer, U.S. Schubert, Poly(ethylene glycol) in drug delivery: Pros and cons as well as potential alternatives, Angew. Chemie - Int. Ed. 49 (2010) 6288–6308. doi:10.1002/anie.200902672.

[12] C.A. Dreiss, E. Nwabunwanne, R. Liu, N.J. Brooks, Assembling and de-assembling micelles: Competitive interactions of cyclodextrins and drugs with Pluronics, Soft Matter. 5 (2009) 1888–1896. doi:10.1039/b812805g.

[13] A. V. Kabanov, E. V. Batrakova, V.Y. Alakhov, Pluronic® block copolymers for overcoming drug resistance in cancer, Adv. Drug Deliv. Rev. 54 (2002) 759–779. doi:10.1016/S0169-409X(02)00047-9.
[14] G. Sahay, E. V. Batrakova, A. V. Kabanov, Different internalization pathways of polymeric micelles and unimers and their effects on vesicular transport, Bioconjug. Chem. 19 (2008) 2023–2029. doi:10.1021/bc8002315.
[15] T. Minko, E. V. Batrakova, S. Li, Y. Li, R.I. Pakunlu, V.Y. Alakhov, A. V. Kabanov, Pluronic block copolymers alter apoptotic signal transduction of doxorubicin in drug-resistant cancer cells, J. Control. Release. 105 (2005) 269–278. doi:10.1016/j.jconrel.2005.03.019.
[16] M. Bohorquez, C. Koch, T. Trygstad, N. Pandit, A Study of the Temperature-Dependent Micellization of Pluronic F127, J. Colloid Interface Sci. 216 (1999) 34–40. doi:10.1006/jcis.1999.6273.
[17] S. Bayati, L. Galantini, K.D. Knudsen, K. Schillén, Effects of Bile Salt Sodium Glycodeoxycholate on the Self-Assembly of PEO-PPO-PEO Triblock Copolymer P123 in Aqueous Solution, Langmuir. 31 (2015) 13519–13527. doi:10.1021/acs.langmuir.5b03828.
[18] S. Bayati, C. Anderberg Haglund, N. V. Pavel, L. Galantini, K. Schillén, Interaction between bile salt sodium glycodeoxycholate and PEO-PPO-PEO triblock copolymers in aqueous solution, RSC Adv. 6 (2016) 69313–69325. doi:10.1039/c6ra12514j.
[19] S. Bayati, L. Galantini, K.D. Knudsen, K. Schillén, Complexes of PEO-PPO-PEO triblock copolymer P123 and bile salt sodium glycodeoxycholate in aqueous solution: A small angle X-ray and neutron scattering investigation, Colloids Surfaces A Physicochem. Eng. Asp. 504 (2016) 426–436. doi:10.1016/j.colsurfa.2016.05.096.
[20] V. Patel, D. Ray, A. Bahadur, J. Ma, V.K. Aswal, P. Bahadur, Pluronic®-bile salt mixed micelles, Colloids Surfaces B Biointerfaces. 166 (2018) 119–126. doi:10.1016/j.colsurfb.2018.03.001.
[21] E. Tasca, A. Del Giudice, L. Galantini, K. Schillén, A.M. Giuliani, M. Giustini, A fluorescence study of the loading and time stability of doxorubicin in sodium cholate/PEO-PPO-PEO triblock copolymer mixed micelles, J. Colloid Interface Sci. 540 (2019) 593–601. doi:10.1016/j.jcis.2019.01.075.
[22] S. Chewchuk, T. Boorman, D. Edwardson, A.M. Parissenti, Bile acids increase doxorubicin sensitivity in ABCC1-expressing tumour cells, Sci. Rep. 8 (2018) 1–12. doi:10.1038/s41598-018-23496-y.
[23] B. Porsch, R. Laga, J. Horský, C. Koňák, K. Ulbrich, Molecular Weight and Polydispersity of Calf-Thymus DNA: Static Light-Scattering and Size-Exclusion Chromatography with Dual Detection, Biomacromolecules. 10 (2009) 3148–3150. doi:10.1021/bm900768j.
[24] M.S. Ibrahim, Voltammetric studies of the interaction of nogalamycin antitumor drug with DNA, Anal. Chim. Acta. 443 (2001) 63–72. doi:10.1016/S0003-2670(0)01184-9.
[25] K.K. Karukstis, E.H.Z. Thompson, J.A. Whiles, R.J. Rosenfeld, Deciphering the fluorescence signature of daunomycin and doxorubicin, Biophys. Chem. 73 (1998) 249–263. doi:10.1016/S0301-4622(98)00150-1.
[26] D. Franke, M. V. Petoukhov, P. V. Konarev, A. Panjkovich, Computer programs ATSAS 2.8: a comprehensive data analysis suite for small-angle scattering from macromolecular solutions, J. Appl. Crystallogr. 50 (2017) 1212–1225. doi:10.1107/S1600576717007786.
[27] http://www.sasview.org/, (n.d.).
[28] M. Airoldi, G. Barone, G. Gennaro, A.M. Giuliani, M. Giustini, Interaction of doxorubicin with polynucleotides. a spectroscopic study, Biochemistry. 53 (2014) 2197–2207. doi:10.1021/bi401687v.

[29] F. Fathian kolahkaj, K. Derakhshandeh, F. Khaleseh, A.H. Azandaryani, K. Mansouri, M. Khazaei, Active targeting carrier for breast cancer treatment: Monoclonal antibody conjugated epirubicin loaded nanoparticle, J. Drug Deliv. Sci. Technol. 53 (2019). doi:10.1016/j.jddst.2019.101136.
[30] M. Tariq, S. Thomas, A. Singh, S. Talegaonkar, Developed and validated stability indicating HPLC method for the determination of epirubicin in bulk drug, marketed injection and polymeric nanoparticles, Brazilian J. Pharm. Sci. 54 (2018). doi:10.1590/s2175-97902018000417515.
[31] R.A. Petras, P.A. Ropp, J.M. DeSimone, Reductively labile PRINT particles for the delivery of doxorubicin to HeLa cells, J. Am. Chem. Soc. 130 (2008) 5008–5009. doi:10.1021/ja801436j.
[32] D.H. Nguyen, J.W. Bae, J.H. Choi, J.S. Lee, K.D. Park, Bioreducible cross-linked Pluronic micelles: PH-triggered release of doxorubicin and folate-mediated cellular uptake, J. Bioact. Compat. Polym. 28 (2013) 341–354. doi:10.1177/0883911513491642.
[33] C.H. Lillig, M.E. Lönn, M. Enoksson, A.P. Fernandes, A. Holmgren, Short interfering RNA-mediated silencing of glutaredoxin 2 increases the sensitivity of HeLa cells toward doxorubicin and phenylarsine oxide, Proc. Natl. Acad. Sci. U. S. A. 101 (2004) 13227–13232. doi:10.1073/pnas.0401896101.
[34] G. Du, H. Lin, M. Wang, S. Zhang, X. Wu, L. Lu, L. Ji, L. Yu, Quercetin greatly improved therapeutic index of doxorubicin against 4T1 breast cancer by its opposing effects on HIF-1α in tumor and normal cells, Cancer Chemother. Pharmacol. 65 (2010) 277–287. doi:10.1007/s00280-009-1032-7.
[35] L. Zhao, L. Zhu, F. Liu, C. Liu, Q. Wang, C. Zhang, J. Li, J. Liu, X. Qu, Z. Yang, pH triggered injectable amphiphilic hydrogel containing doxorubicin and paclitaxel, Int. J. Pharm. 410 (2011) 83–91. doi:10.1016/j.ijpharm.2011.03.034.
[36] D. Zhang, L. Tao, H. Zhao, H. Yuan, M. Lan, A functional drug delivery platform for targeting and imaging cancer cells based on Pluronic F127, J. Biomater. Sci. Polym. Ed. 26 (2015) 468–482. doi:10.1080/09205063.2015.1030136.
[37] Z. Wei, J. Hao, S. Yuan, Y. Li, W. Juan, X. Sha, X. Fang, Paclitaxel-loaded Pluronic P123/F127 mixed polymeric micelles: Formulation, optimization and in vitro characterization, Int. J. Pharm. 376 (2009) 176–185. doi:10.1016/j.ijpharm.2009.04.030.
[38] X. Zeng, R. Morgenstern, A.M. Nyström, Nanoparticle-directed sub-cellular localization of doxorubicin and the sensitization breast cancer cells by circumventing GST-Mediated drug resistance, Biomaterials. 35 (2014) 1227–1239. doi:10.1016/j.biomaterials.2013.10.042.
[39] P. Dehghankelishadi, E. Saadat, F. Ravar, M. Safavi, M. Pordeli, M. Gholami, F.A. Dorkoosh, In vitro and in vivo evaluation of paclitaxel–lapatinib-loaded F127 pluronic micelles, Drug Dev. Ind. Pharm. 43 (2017) 390–398. doi:10.1080/03639045.2016.1254238.
[40] H. Sun, Q. Meng, S. Tang, J. Su, Q. Yin, L. Chen, W. Gu, H. Yu, Z. Zhang, S. Wang, Y. Li, Inhibition of Breast Cancer Metastasis by Pluronic Copolymers with Moderate Hydrophilic-Lipophilic Balance, Mol. Pharm. 12 (2015) 3323–3331. doi:10.1021/acs.molpharmaceut.5b00319.
[41] X. Dai, Z. Yue, M.E. Eccleston, J. Swartling, N.K.H. Slater, C.F. Kaminski, Fluorescence intensity and lifetime imaging of free and micellar-encapsulated doxorubicin in living cells, Nanomedicine Nanotechnology, Biol. Med. 4 (2008) 49–56. doi:10.1016/j.nano.2007.12.002.
[42] A. Sahu, N. Kasoju, P. Goswami, U. Bora, Encapsulation of curcumin in Pluronic block copolymer micelles for drug delivery applications, J. Biomater. Appl. 25 (2011) 619–

639. doi:10.1177/0885328209357110.
[43] Z. Wei, S. Yuan, J. Hao, X. Fang, Mechanism of inhibition of P-glycoprotein mediated efflux by Pluronic P123/F127 block copolymers: Relationship between copolymer concentration and inhibitory activity, Eur. J. Pharm. Biopharm. 83 (2013) 266–274. doi:10.1016/j.ejpb.2012.09.014.
[44] W. Fan, X. Wu, B. Ding, J. Gao, Z. Cai, W. Zhang, D. Yin, X. Wang, Q. Zhu, J. Liu, X. Ding, S. Gao, Degradable gene delivery systems based on Pluronics-modified low-molecular-weight polyethylenimine: Preparation, characterization, intracellular trafficking, and cellular distribution, Int. J. Nanomedicine. 7 (2012) 1127–1138. doi:10.2147/IJN.S27117.
[45] M. Valero, F. Castiglione, A. Mele, M.A. Da Silva, I. Grillo, G. González-Gaitano, C.A. Dreiss, Competitive and Synergistic Interactions between Polymer Micelles, Drugs, and Cyclodextrins: The Importance of Drug Solubilization Locus, Langmuir. 32 (2016) 13174–13186. doi:10.1021/acs.langmuir.6b03367.